Original research article

IJAO The International Journal of Artificial Organs

Effects of the atrium on intraventricular flow patterns during mechanical circulatory support

The International Journal of Artificial Organs
2022, Vol. 45(4) 421–430

DOI: 10.1177/03913988211056018
journals.sagepub.com/home/jao


Mojgan Ghodrati[1,2], Thomas Schlöglhofer[1,2,3], Alexander Maurer[1,2], Thananya Khienwad[1], Daniel Zimpfer[3], Dietrich Beitzke[4], Francesco Zonta[5], Francesco Moscato[1,2], Heinrich Schima[1,2,3] and Philipp Aigner[1,2]

Abstract

Simulations of the ventricular flow patterns during left ventricular assist device (LVAD) support are mainly performed with idealized cylindrical inflow, neglecting the influence of the atrial vortex. In this study, the influence of the left atrium (LA) on the intra-ventricular flow was investigated via Computational Fluid Dynamics (CFD) simulations. Ventricular flow was simulated by a combined Eulerian (carrier flow)/Lagrangian (particles) approach taking into account either the LA or a cylindrical inflow section to mimic a fully support condition. The flow deviation at the mitral valve, the blood low-velocity volume as well as the residence time and shear stress history of the particles were calculated. Inclusion of the LA deflects the flow at the mitral valve by 25°, resulting in an asymmetric flow jet entering the left ventricle. This reduced the ventricular low-velocity volume by 40% (from 6.4 to 3.9 cm^3), increased (40%) the shear stress experienced by particles and correspondingly increased (27%) their residence time. Under the studied conditions, the atrial geometry plays a major role in the development of intraventricular flow patterns. A reliable prediction of blood flow dynamics and consequently thrombosis risk analysis within the ventricle requires the consideration of the LA in computational simulations.

Keywords

Left ventricle assist device, intraventricular flow pattern, left atrium, computational fluid dynamics, shear stress history, residence time

Date received: 26 May 2021; accepted: 6 October 2021

Introduction

The prevalence of heart failure increases over time with an aging population affecting at least 26 million people worldwide.[1] In patients with advanced heart failure, heart transplantation is known as a standard therapy[2,3] but Left Ventricular Assist Devices (LVADs) are being considered as an alternative treatment for these patients due to the limited number of heart donors.[4] Despite the success of this treatment[5] there is still a high risk of thrombosis and consequently a high mortality rate from stroke.[6,7] Non-physiological intraventricular flow dynamics[8,9] caused by LVADs such as stasis and high shear stresses have been known as the risk factors for thrombosis.[10,11]

[1]Center for Medical Physics and Biomedical Engineering, Medical University of Vienna, Vienna, Austria
[2]Ludwig Boltzmann Institute for Cardiovascular Research, Vienna, Austria
[3]Department of Cardiac Surgery, Medical University of Vienna, Vienna, Austria
[4]Department of Biomedical Imaging and Image guided Therapy, Medical University of Vienna, Vienna, Austria
[5]Institute of Fluid Dynamics and Heat Transfer, Technical University of Vienna, Vienna, Austria

Corresponding author:
Philipp Aigner, Center for Medical Physics and Biomedical Engineering, Medical University of Vienna, Währinger Gürtel 18-20, AKH-4L, Vienna 1090, Austria.
Email: philipp.aigner@meduniwien.ac.at

Computational Fluid Dynamics (CFD) studies proved that unfavorable LVAD-related hemodynamics and thrombosis risk could be reduced if an optimal cannula position is chosen. Reduction in the stasis and consequently better blood washout was associated with the apical placement of the cannula compared to diaphragmatic positioning.[12] Also lower stasis was observed with the longer insertion length when different cannula insertion depth were compared.[13] The impact of the inflow cannula angle with respect to the mitral-apex axis revealed significant reduction in thrombosis risk when inflow angulation was within $0 \pm 7°$.[14]

Although numerical simulations can be a useful tool for flow field analysis and for evaluation of the critical parameters at the location of depositions, the accuracy of the simulated flow fields is highly dependent on the defined inflow conditions. It was shown that the predicted ventricular flow patterns in the healthy heart can vary significantly if different boundary conditions are imposed at the mitral valve.[15]

The typical mitral flow condition for LVAD assisted ventricle is the straight flow direction at the mitral valve created by a cylindrical inflow (Figure 1(a)) which is considered instead of the Left Atrium (LA) (Figure 1(b)).

However, 4D Flow MRI visualization show that the in vivo blood flow pattern within the left atrium develops a different flow pattern at the mitral valve than a straight flow created by a simplified cylindrical inflow.[16] Interaction of the blood flowing from the left and right PV leads to formation of the vortex at the center of the LA[17] developing an asymmetric flow jet at the MV.[16] This velocity profile was not replicable by cylindrical inflow and therefore leads to inaccurate ventricular flow prediction than the clinical in vivo measurements.[16] This evaluation was performed for the healthy heart and has not been studied yet for the LVAD assisted ventricle.

In this study the effects of the left atrium on ventricular flow fields in LVAD patients was investigated using CFD simulations of individual patient geometries with and without the left atrium.

Materials and methods

Patient models

The left heart (LH) and the pump of an LVAD patient (male, 75 years, BMI: 32.7 kg/m^2 Intermacs level: 4) suffering from dilated cardiomyopathy was segmented at end systole from computed tomography (CT) images using Mimics Research 20.0 and 3-matics Research 13.0 (Materialise, Belgium NV), including the structures of the left atrium (volume 250 ml) and left ventricle (volume 264 ml). The image segmentation and preparation post-processing of the geometry was performed under the guidance and supervision of a radiologist.

For the first simulation, a 30 mm diameter cylinder that served as a simplified representation of the LA geometry (Figure 1(a)) was attached to the LV, constituting the typical approach used in previous CFD studies for LVAD patients.[13,14,18,19] The size of the cylinder (30 mm) corresponds to the size of the mitral annulus deriving from CT-scan and placed in the position of the mitral valve which also derived from CT data. In the second simulation, the anatomical LA was included (Figure 1(b)). The geometry of the HeartWare HVAD (Medtronic, Minneapolis, MN) inflow cannula was considered in this study and it was placed into the model in ANSYS, SpaceClaim (Ansys 19.1, Pennsylvania, USA). In order to have the most realistic scenario for inflow cannula placement, position, and direction of the inflow cannula was derived from CT scans.

Meshing

An unstructured tetrahedral mesh with total 2.4 million cells for the LA and 3.0 million cells for LV was created (ANSYS Meshing 19.1, Pennsylvania, US). The suitable mesh size was chosen based on a mesh independence study which can be found in Supplemental Appendix. All of the mesh elements had a skewness below 0.84 and orthogonal quality above 0.16 which is in the recommended ranges, refer to the Ansys Meshing User Guide.[20]

Boundary conditions and solver setting

The Navier-Stokes equations were solved using the finite-volume CFD solver (FLUENT, Ansys 19.1, Pennsylvania, USA). The presence of turbulence structure within the left heart has been a matter of debate and many CFD studies considered the Laminar flow regime within the LA and LV.[13,18,21] Note that the average Reynolds number during cardiac cycle calculated at the pulmonary veins was 830 with a short period of 2500 at the peak E-wave and A-wave. In a previous study, the laminar method showed better agreement with the experimental results of ventricular flow fields compared to the turbulence models.[22] As a consequence, blood was here assumed a Newtonian fluid—with a density of 1060 kg/m^3 and a dynamic viscosity of 0.0035 Pa s—and in laminar conditions.

Simulations were performed for the duration of 9 Cardiac Cycles (CC) and with a time step of 0.001 s which was chosen based on the aforementioned study.[22] Convergence was considered in each time step when the residuals were below 10^{-3} for continuity, x-velocity, y-velocity, and z-velocity, refer to recommended value in ANSYS Fluent User Guide.[23] The simulations had an initialization time of 5 s with a constant flow rate of 5 L/min to ensure the full flow development within the left heart.

The inflow waveform (Figure 1(c)) was derived by lumped parameter network model simulation of a

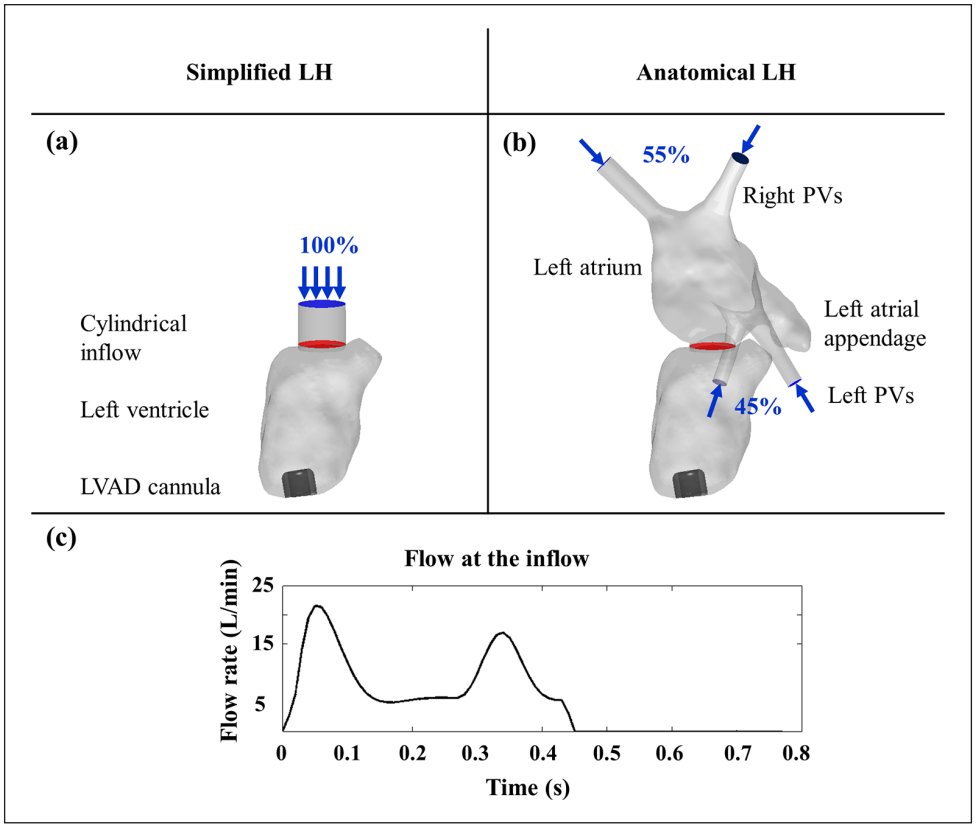

Figure 1. (a) Patient-specific left heart including cylindrical inflow and left ventricle. (b) Anatomical left heart including pulmonary veins (PVs), left atrium and left ventricle. (Red surface shows the location of the particle injection.) (c) Blood flow rate through the mitral valve and PVs over one cardiac cycle.

typical LVAD patient[24] with dilated left ventricle and ejection fraction less than 20%. Given very low ejection fraction which leads to minimal ventricular variation in systole versus diastole the geometry was modeled as rigid.

For the simplified LH the flow rate with the uniform profile was assigned at the inlet of the cylinder (Figure 1(a)). For the anatomical LH it was applied at the pulmonary veins replicating the ratio of the peaks of the two pulmonary veins inflow phases observed by previous studies.[25–27] The flow rate was distributed with a portion of 55% from right PVs (27.5% each PV), and 45% from left PVs (22.5% each PV),[28] (Figure 1(b)). The mass-flow rate boundary condition was applied at the pulmonary veins and outflow boundary conditions were imposed at the LVAD cannula. Outflow is a type of outlet boundary conditions in Fluent (Ansys 19.1, Pennsylvania, USA) and used to model flow exits.[23]

A Lagrangian approach was used to track 10,000 massless particles with a diameter of 3 μm[19]. Particles were injected every 0.01 s over the first cardiac cycle at the MV annulus (Figure 1(a) and (b), red plane). The particles were then tracked over nine cardiac cycles within the LV which allowed us to evaluate particles behavior over time in a cumulative manner.

The risk of platelet activation and aggregation was evaluated by analysis of particle trajectories inside of the LV. The Shear Stress Histories (SSH), equation (1), and the Residence Times (RT) of the particles, equation (2), were used as indicators for thrombogenicity.[14,18]

Shear Stress History

$$SSH = \int_{t_0}^{t} \tau\left(X\left(t'\right), t'\right) dt' \tag{1}$$

Residence Time

$$RT_i = T_i^{entrance} - T_i^{exit} \tag{2}$$

Note that t_0 is the time when particles enter the LV, t is the time when particles leave the LV, τ is the instantaneous shear stress, $X\left(t'\right)$ is the location of each particle at time t', i is the particle number, $T_i^{entrance}$ is the time at which particles enter the LV and T_i^{exit} is the time at which particles leave the LV.

Statistical analysis

Descriptive statistics are presented as mean ± standard deviation (SD) for continuous variables and number

(percentage) for categorical variables. Where continuous variables were non-normally distributed, data is presented as median and interquartile range (IQR). Normal distribution was assessed by the Kolmogorov-Smirnov test. Particle residence time and shear stress history of the two groups (simplified LH and anatomical LH) were compared using the independent *t*-test for continuous data or the Mann-Whitney *U*-test for data that were not normally distributed. Changes of particle shear stress history over time (from CC1 to CC9) were analyzed by non-parametric Friedman test; post hoc analysis with Wilcoxon signed-rank tests was conducted with a Bonferroni correction applied. Statistical analysis was performed using SPSS for Windows Release 26.0.0 (SPSS Inc., Chicago, IL) and Matlab R2017b (The MathWorks Inc.). Statistical significance was set at $p < 0.05$.

This analysis was performed beatwise to compare the shear stress in cumulative fashion, since particles with longer residence time accumulate shear values for longer period which increase the risk of platelet activation.

Flow parameter evaluation

The flow field was visualized using time-averaged velocities over 9CC. The intra-ventricular flow fluctuations were calculated using root mean square of the fluctuating velocity.

The deviation of the flow at the mitral valve was measured at the MV using equation (3).

$$\Delta\theta = \cos^{-1}\left(\frac{\bar{a}.\bar{b}}{|\bar{a}|.|\bar{b}|}\right) \quad (3)$$

In which $\bar{a}$ and $\bar{b}$ are the 3D time-averaged velocity vectors over 9CC at the mitral valve for a simplified and an anatomical LH, respectively.

Two established measures were used in this study to evaluate the risk of thromboembolism, due to the fact that platelet activation and consequently thrombosis is a multifactorial phenomenon. The first one is related to regions with low-velocity[10,29–31] and wall shear stress (WSS)[32–34] and highlights the local regions with a high risk of platelet deposition and the near-wall thrombus growth. While the second one is based on the residence time (RT) and shear stresses history (SSH) of each particle[14,18,35] and evaluate the risk of platelet activation within the whole LV.

Time averaged WSS over 9CC at the LA wall, LV wall and inflow cannula surface was categorized in three levels[36]: low non-physiological range (0–0.2 Pa) which is related to thrombus formation,[32] physiological range (0.2–9 Pa) and high non-physiological range which leads to Von Willebrand Factor (VWF) degradation (>9 Pa).[11]

Blood stasis is one of the three factors introduced by Virchow's triad contributing to thrombosis. However, there is currently no established velocity threshold to define the low-velocity volume. The threshold in this study was chosen to highlight any regions where low time-averaged shear stresses are observed, based on the assumption that any particles traveling above 0 and less than 5 mm/s through the wedge area could possibly result in thrombosis because of clotting mechanisms which are activated at such low shear rates.

The fluid dynamics parameters were evaluated over all 9CC, since the particles were injected at the beginning of the first CC.

Results

Flow structure differed markedly between the cylindrical inflow and the LA model. The cylindrical inflow led to parallel flow streamlines and therefore symmetric flow profile at the MV (Figure 2(a) and (c)). The streamlines within the LA showed the formation of a large vortex at the center of the LA resulting in an asymmetric flow profile at the MV (Figure 2(b) and (d)). The results of intra-atrial flow simulation and atrial vortex is supported by previous studies.[17] In the anatomical model the pulmonary inflow resulted in an atrial vortex, that skewed the inflow from 5° to 36° over a cardiac cycle and in average by 25° at the MV compared to straight flow created by the cylindrical inflow (Figure 2(c) and (d)).

Obvious differences can be seen in the velocity distribution within the LV as a result of the different inflow geometries. The main flow jet of the simplified LH directed to the inflow cannula (Figure 3(a)), while for the anatomical LH it was directed toward the septal wall (Figure 3(b)), leading to higher velocity distribution around the mitral annulus and LVOT. The straight inflow patterns in the simplified LH directed the majority of flow toward the inflow cannula (Figure 3(c)). By contrast, with the anatomical LH the flow streamlines deviated toward the septum downstream of the MV (Figure 3(d)). Therefore, the main flow jet reached the apex of the LV at the septal side, creating higher apical washout (Figure 3(d)).

Evaluation of the fluctuation of the flow fields revealed that beside the flow variations created by pulsatile flow (can be seen within the cylindrical inflow) the geometry of the LA itself plays a crucial role. Inclusion of the anatomical LA imposed higher ventricular flow fluctuations mainly downstream of the MV when compared to the cylindrical inflow (Figure 3(e) and (f)).

For the simplified LH larger low-WSS areas at the Left Ventricular Outflow Tract (LVOT) and at the septal side of the LV apex were found when it compared to anatomical LH (Figure 4(a) and (b)), increasing the area with low WSS for 33% (from 79 to 105 cm^2). Moreover, low non-physiological WSS was observed over the whole wall of the left atrial appendage (Figure 4(c)). On the other end, high non-physiological shear stress was observed only at

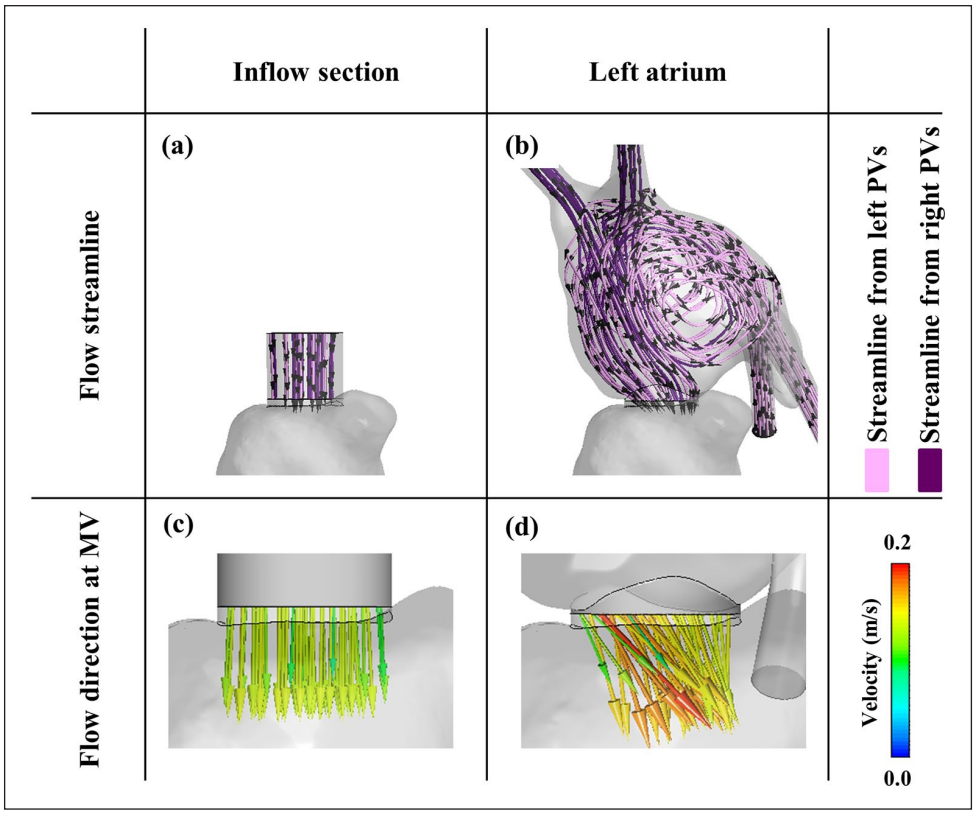

Figure 2. First row (a,b): time-averaged flow streamline over 9CC within the inflow section and the left atrium, second row (c,d): time-averaged velocity vectors over 9CC at the mitral valve without and with enclosure of the left atrium.

the tip of the inflow cannula for both cases (Figure 4(a) and (b)). A large pocket of low-velocity volume was seen at the LVOT and at the septal side of the apex for the simplified model, which was diminished for the anatomical model (Figure 4(d) and (e)). The low-velocity volume around the LVOT was formed as a large pocket, while at the LV apex was composed of some small pockets. In overall, the ventricular low-velocity volume decreased for 40% (from 6.4 to 3.9 cm^3) when cylindrical inflow section was replaced by LA (Figure 4(d) and (e)). A large pocket of low-velocity volume was also formed in the left atrial appendage of the anatomical atrium with some small pockets all over the LA (Figure 4(f)).

Simulation of the particle trajectories revealed that the trajectories with the anatomical LA were longer and more deflected, hence not directly pointing toward the outflow. As a result, after three cardiac cycles 53% of particles approached the LVAD inflow cannula for the simplified model compared to 47% for the anatomic model (Figure 5(a)). After 9CC, 15% more particles remain within the LV for the anatomical model compared to the simplified model (Figure 5(a)).

In the anatomical model particles also experienced higher shear stresses for all cardiac cycles (Figure 5(b) and (c)). The median values of SSH were compared between the two models (with/without LA) over separate cardiac cycles. An increase of 22% to 28% in SSH was observed over 9CC as a result of the inclusion of the anatomical LA. Comparison of the repeated measures (cardiac cycle) showed a statistically significant difference particle shear stress history for the simplified and anatomical model with, $\chi^2(8)=1591.9$, $p<0.001$ and $\chi^2(8)=576.3$, $p<0.001$, respectively. Post hoc analysis with Wilcoxon signed-rank test was conducted with a Bonferroni correction applied, resulting in a significance level set at $p<0.0056$. Investigating changes from one cardiac cycle to the next, a significant increase in particle shear stress history was found in the simplified anatomy between CC1 and CC2 ($Z=-1.28$, $p<0.001$), CC2 and CC3 ($Z=-1.24$, $p<0.001$), CC4 and CC5 ($Z=-0.86$, $p<0.001$), and CC5 and CC6 ($Z=-1.02$, $p<0.001$). In the anatomical model, however, shear stress history increased significantly only between CC6 and CC7 ($Z=-1.45$, $p=0.001$).

Moreover, the overall analysis of RT and SSH over nine cardiac cycles revealed that particles experienced 40% more shear stress as well as 27% longer residence time with the anatomical LA which were calculated from median values (Table 1).

Discussion

Implantation of a LVAD creates non-physiological flow patterns within the LV, which might lead to thrombus formation and consequently to thromboembolic and

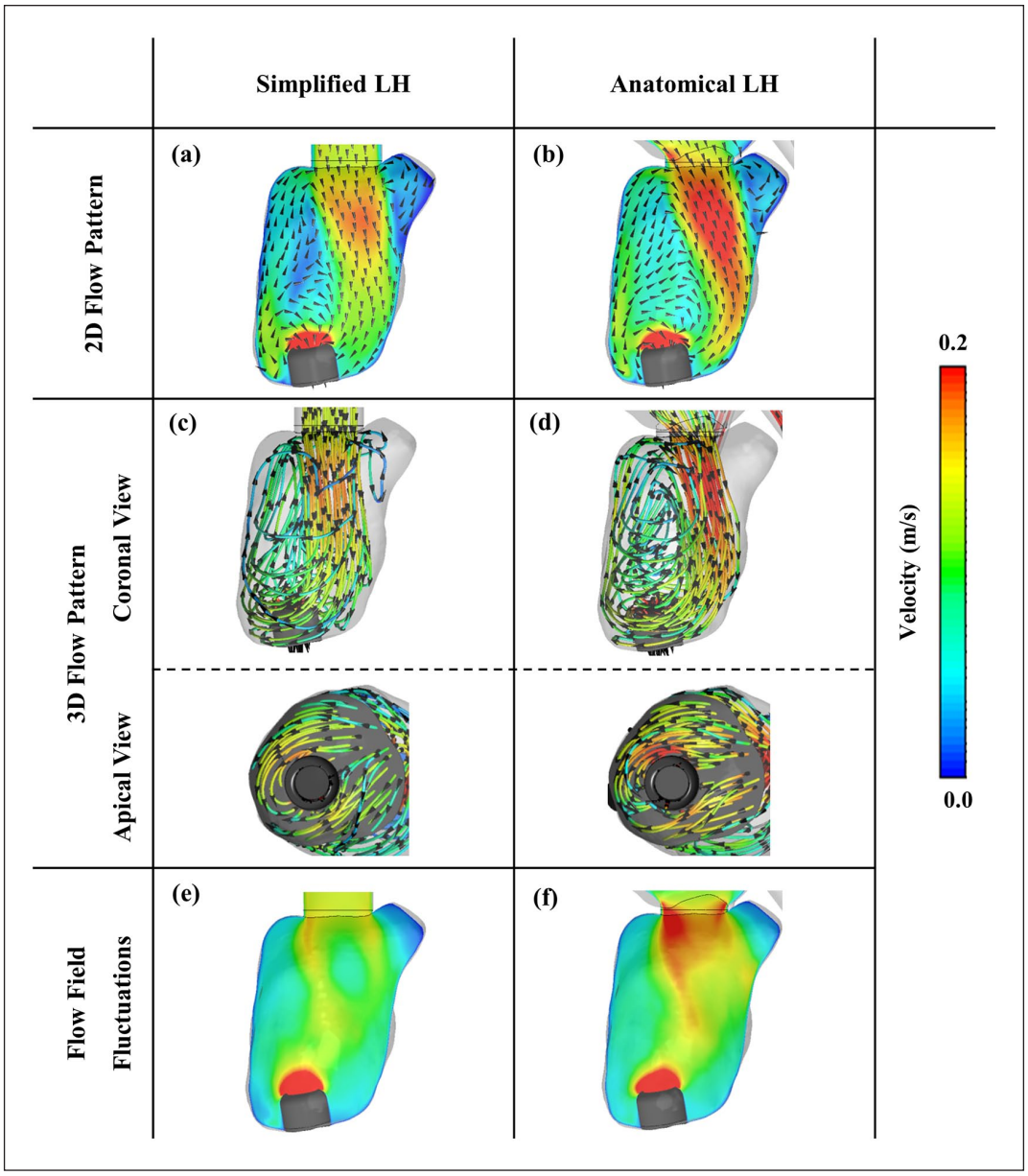

Figure 3. First row (a,b): time-averaged 2D ventricular flow pattern at the mid-coronal plane over 9CC. Second row (c,d): time-averaged 3D ventricular flow pattern over 9CC. Third row (e,f): flow field fluctuations for the simplified and anatomical LH at the mid-coronal plane over 9CC.

neurological adverse events.[6,7,37] This highlights a strong need for evaluation of the intraventricular hemodynamics and flow dynamics to minimize the thrombosis risk and ultimately improve the clinical outcome of LVAD therapy.

Cardiac imaging techniques in LVAD patients are still limited.[38] Therefore, CFD simulations are a useful tool to provide insights into ventricular flow fields and to evaluate thrombosis-related parameters during LVAD support. However, the accuracy and reliability of CFD simulations heavily depends on the correct choice of boundary conditions.

Previous CFD studies for LVAD-supported ventricles were usually performed with a cylindrical inflow section[13,14,18,19,39] which creates the situation of a straight symmetric flow profile at the MV (Figure 2(c)). This symmetric mitral flow results in more direct blood flow from the MV to the inflow cannula (Figure 3(c)), creating lower washout and consequently larger low-velocity volume at the apex and LVOT when compared to the anatomical LH simulation (Figure 4). While the prediction of possible thrombus deposition locations was not the aim of this study, it was shown that inaccurate simulation of the blood stasis region could result in misprediction of these

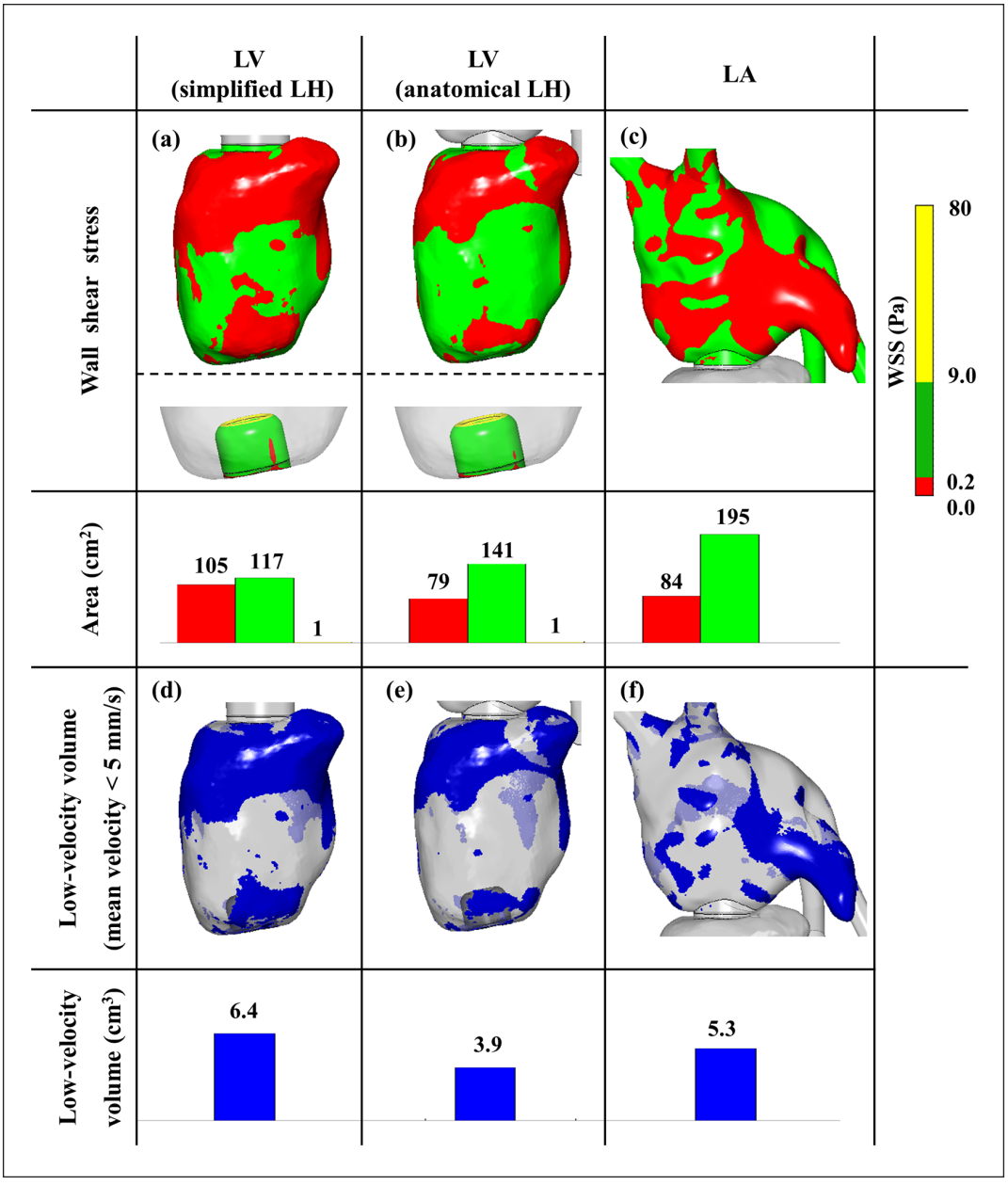

Figure 4. First row (a,b,c): Time-averaged wall shear stress distribution at the ventricular wall, inflow cannula surface, and atrial wall. Second row (d,e,f): time-averaged low-velocity volume within the ventricle and atrium for the simplified and anatomical LH.

aforementioned regions with low-velocity. The inclusion of the LA geometry is therefore probably necessary in future studies if the thrombosis risk is going to be investigated.

By consideration of the LA in the simulation, the well-known atrial vortex was formed at the center of the LA which deviated from the blood flow direction at the MV by 25° compared to the simplified inflow (Figure 2). This deviation strongly influenced the flow path within the ventricle, directing a major part of the flow toward the septum instead of the inflow cannula. As a consequence, blood particles developed longer and more convoluted trajectories, leading to higher median residence time. This behavior was different from the simplified LH, where most particles had a shorter path to the inflow cannula with less residence time (Table 1). Further, inclusion of the anatomical left atrium resulted in an overall significant increase in SSH values (Table 1) and a larger proportion of the particles experienced exposure to high RT, indicating elevated risk of platelet activation and thrombus formation.

Moreover, consideration of the anatomical LA provides helpful information regarding the atrial flow field and stasis within the left atrial appendage. Clinical data showed

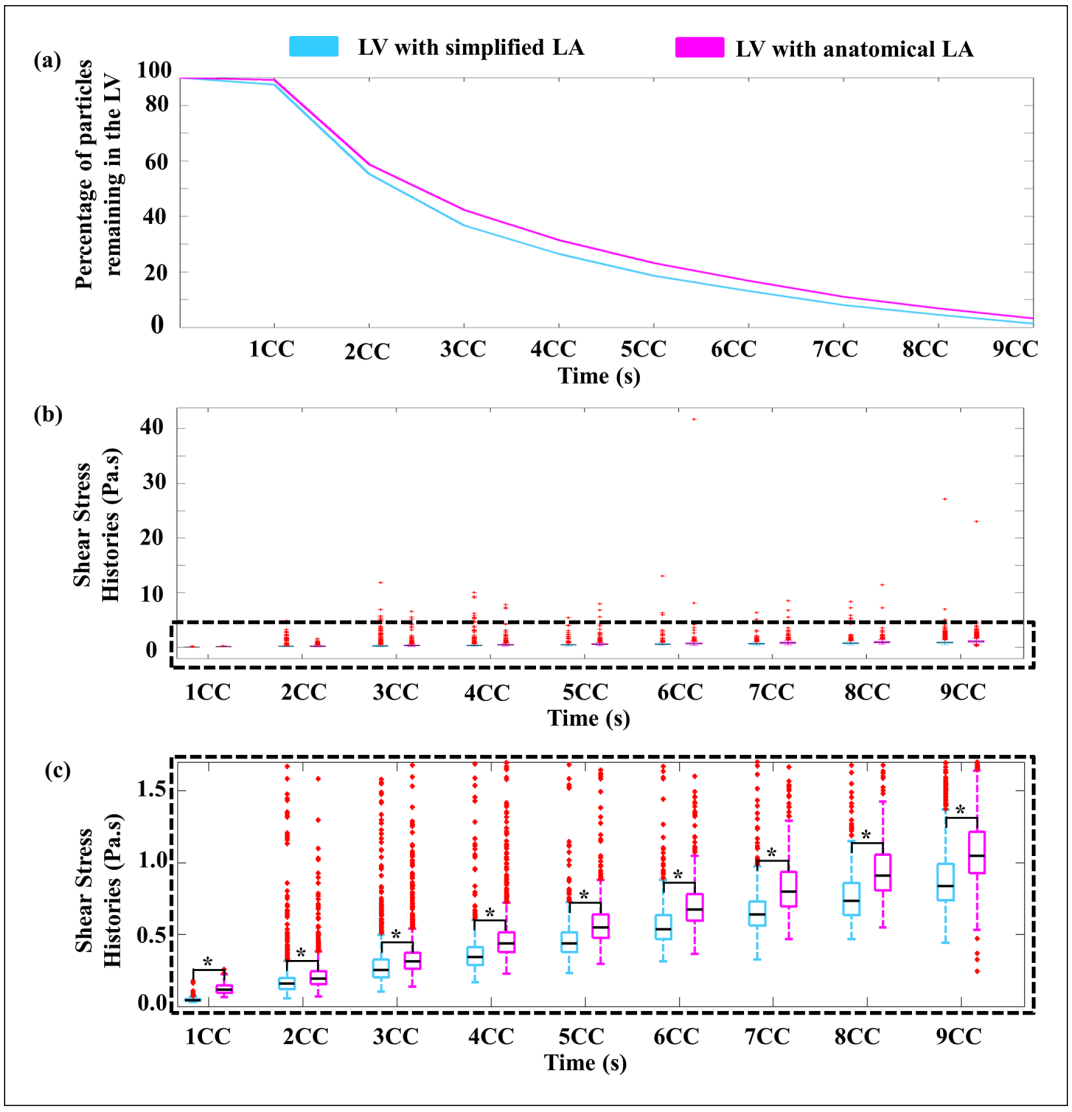

Figure 5. First row (a): percentage of the particles that remains in LV. Second (b) and third (c) rows: box plots of particles shear stress history at each cardiac cycle.
*Indicates significant difference.

Table 1. Statistical analysis of the particle residence time (RT) and shear stress history (SSH) values for all particles.

	Simplified LH (n = 10,000)	Anatomical LH (n = 10,000)	p-Value
Particle residence time (s)	1.89 (3.09)	2.40 (3.65)	<0.001
Particle shear stress history (Pa s)	0.30 (0.42)	0.42 (0.56)	<0.001

Data presented as median (IQR).

that the atrial appendage could be a source of thrombus in patients with LVAD[40] and its occlusion was associated with reduced thromboembolic events.[41]

Limitation

Due to our study design, several limitations are unavoidable and shall not remain unmentioned. This study was performed for a single patient and needs to be increased in the future studies to include different types of the LA. However, it is expected that the inclusion of the LA in general results in different ventricular flow fields and particle trajectories.

The contractility of the left atrium was not considered in this study. However, the key feature of the intra-atrial flow, the atrial vortex,[42] was successfully simulated.

Additionally the ventricular flow patterns and vortex formation is mainly driven by the diastolic inflow as previous studies showed.[43]

The mitral valve was not considered in the current model. Although the left atrium and mitral valve have complementary effects on ventricular flow development, only the left atrium was considered in this study. The mitral valve geometry has an influence on ventricular vortex development[44–46] and needs to be considered in future studies. In summary, we consider this study as a step toward accurate intra-ventricular flow simulation for LVAD patients.

Conclusion

The geometry of the left atrium and flow from the pulmonary veins play a significant role in the development of the ventricular blood flow dynamics. Therefore, reliable prediction of local blood for stasis and thrombosis risk assessment within the LV and recommendation for the optimal surgical configuration of LVAD devices based on CFD simulations requires consideration of the LA.

Declaration of conflicting interests

The author(s) declared the following potential conflicts of interest with respect to the research, authorship, and/or publication of this article: Daniel Zimpfer has served as a proctor, advisor, and speaker for Medtronic Inc., Abbott Inc., Berlin Heart, Edwards, Abiomed, and has received research and travel grants from Medtronic Inc. and Abbott Inc. Heinrich Schima has served as an advisor for Medtronic Inc. and has received research grants from Medtronic Inc. Thomas Schlöglhofer has served as a consultant and advisor for Medtronic Inc. and Abbott Inc. All other authors have nothing to disclose.

Funding

The author(s) disclosed receipt of the following financial support for the research, authorship, and/or publication of this article: This work was supported by the Vienna Scientific Cluster (VSC) Computer Network, the Project of the Jubiläumsfonds of the National Bank Austria Nr. 17314 and the Austrian Research Promotion Agency (FFG): M3dRES Project Nr. 858060.

ORCID iDs

Dietrich Beitzke https://orcid.org/0000-0003-3179-3827
Philipp Aigner https://orcid.org/0000-0002-3212-2112

Supplemental material

Supplemental material for this article is available online.

References

1. Savarese G and Lund LH. Global public health burden of heart failure. *Card Fail Rev* 2017; 3(1): 7–11.
2. Theochari CA, Michalopoulos G, Oikonomou EK, et al. Heart transplantation versus left ventricular assist devices as destination therapy or bridge to transplantation for 1-year mortality: a systematic review and meta-analysis. *Ann Cardiothorac Surg* 2018; 7(1): 3–11.
3. Haeck ML, Hoogslag GE, Rodrigo SF, et al. Treatment options in end-stage heart failure: where to go from here? *Neth Heart J* 2012; 20(4): 167–175.
4. Mancini D and Colombo PC. Left ventricular assist devices: a rapidly evolving alternative to transplant. *J Am Coll Cardiol* 2015; 65(23): 2542–2555.
5. Kirklin JK, Pagani FD, Kormos RL, et al. Eighth annual INTERMACS report: special focus on framing the impact of adverse events. *J Heart Lung Transplant* 2017; 36(10): 1080–1086.
6. Acharya D, Loyaga-Rendon R, Morgan CJ, et al. INTERMACS analysis of stroke during support with continuous-flow left ventricular assist devices: risk factors and outcomes. *JACC Heart Fail* 2017; 5(10): 703–711.
7. DeVore AD and Stewart GC. The risk of stroke on left ventricular assist device support: steady gains or stalled progress? *JACC Heart Fail* 2017; 5(10): 712–714.
8. Aigner P, Schweiger M, Fraser K, et al. Ventricular flow field visualization during mechanical circulatory support in the assisted isolated beating heart. *Ann Biomed Eng* 2020; 48(2): 794–804.
9. Reider C, Moon J, Ramesh V, et al. Intraventricular thrombus formation in the LVAD-assisted heart studied in a mock circulatory loop. *Meccanica* 2017; 52(3): 515–528.
10. Lowe GDO. Virchow's triad revisited: abnormal flow. *Pathophysiol Haemost Thromb* 2003; 33(5–6): 455–457.
11. Fraser KH, Zhang T, Taskin ME, et al. A quantitative comparison of mechanical blood damage parameters in rotary ventricular assist devices: shear stress, exposure time and hemolysis index. *J Biomech Eng* 2012; 134(8): 081002.
12. Prisco AR, Aliseda A, Beckman JA, et al. Impact of LVAD implantation site on ventricular blood stagnation. *ASAIO J* 2017; 63(4): 392–400.
13. Liao S, Neidlin M, Li Z, et al. Ventricular flow dynamics with varying LVAD inflow cannula lengths: in-silico evaluation in a multiscale model. *J Biomech* 2018; 72: 106–115.
14. Chivukula VK, Beckman JA, Prisco AR, et al. Left ventricular assist device inflow cannula angle and thrombosis risk. *Circ Heart Fail* 2018; 11(4): e004325.
15. Long Q, Merrifield R, Yang GZ, et al. The influence of inflow boundary conditions on intra left ventricle flow predictions. *J Biomech Eng* 2003; 125(6): 922–927.
16. Schenkel T, Malve M, Reik M, et al. MRI-Based CFD analysis of flow in a human left ventricle: methodology and application to a healthy heart. *Ann Biomed Eng* 2009; 37(3): 503–515.
17. Fyrenius A, Wigström L, Ebbers T, et al. Three dimensional flow in the human left atrium. *Heart* 2001; 86(4): 448–455.
18. Chivukula VK, Beckman JA, Prisco AR, et al. Small left ventricular size is an independent risk factor for ventricular assist device thrombosis. *ASAIO J* 2019; 65(2): 152–159.
19. Sonntag SJ, Lipinski E, Neidlin M, et al. Virtual fitting and hemodynamic simulation of the EVAHEART 2 left ventricular assist device and double-cuff tipless inflow cannula. *ASAIO J* 2019; 65: 698–706.
20. Baker TJ. *ANSYS fluent meshing user's guide*, Release 17.0, Jan 2016.

21. Bosi GM, Cook A, Rai R, et al. Computational fluid dynamic analysis of the left atrial appendage to predict thrombosis risk. *Front Cardiovasc Med* 2018; 5: 34.
22. Ghodrati M, Khienwad T, Maurer A, et al. Validation of numerically simulated ventricular flow patterns during left ventricular assist device support. *Int J Artif Organs* 2021; 44: 30–38.
23. Ahmad T, Plee SL and Myers JP. *Fluent user's guide*, Release 17.0, Jan 2016.
24. Moscato F, Granegger M, Naiyanetr P, et al. Evaluation of left ventricular relaxation in rotary blood Pump recipients using the pump flow waveform: a simulation study. *Artif Organs* 2012; 36(5): 470–478.
25. Keren G, Sherez J, Megidish R, et al. Pulmonary venous flow pattern—its relationship to cardiac dynamics. A pulsed Doppler echocardiographic study. *Circulation* 1985; 71(6): 1105–1112.
26. Nishimura RA, Abel MD, Hatle LK, et al. Relation of pulmonary vein to mitral flow velocities by transesophageal Doppler echocardiography. Effect of different loading conditions. *Circulation* 1990; 81(5): 1488–1497.
27. Liang F and Liu H. A closed-loop lumped parameter computational model for human cardiovascular system. *JSME Int J C* 2005; 48(4): 484–493.
28. Wong DT, Lee K-J, Yoo S-J, et al. Changes in systemic and pulmonary blood flow distribution in normal adult volunteers in response to posture and exercise: a phase contrast magnetic resonance imaging study. *J Physiol Sci* 2014; 64(2): 105–112.
29. May-Newman K, Wong YK, Adamson R, et al. Thromboembolism is linked to intraventricular flow stasis in a patient supported with a left ventricle assist device. *ASAIO J* 2013; 59(4): 452–455.
30. Méndez Rojano R, Zhussupbekov M and Antaki JF. Multiconstituent simulation of thrombus formation at LVAD inlet cannula connection: importance of Virchow's triad. *Artif Organs* 2021; 45: 1014–1023.
31. Rayz VL, Boussel L, Lawton MT, et al. Numerical modeling of the flow in intracranial aneurysms: prediction of regions prone to thrombus formation. *Ann Biomed Eng* 2008; 36(11): 1793–1804.
32. Rayz VL, Boussel L, Ge L, et al. Flow residence time and regions of intraluminal thrombus deposition in intracranial aneurysms. *Ann Biomed Eng* 2010; 38(10): 3058–3069.
33. Wu WT, Jamiolkowski MA, Wagner WR, et al. Multiconstituent simulation of thrombus deposition. *Sci Rep* 2017; 7(1): 42720.
34. Inauen W, Baumgartner HR, Bombeli T, et al. Dose- and shear rate-dependent effects of heparin on thrombogenesis induced by rabbit aorta subendothelium exposed to flowing human blood. *Arteriosclerosis* 1990; 10(4): 607–615.
35. Einav S and Bluestein D. Dynamics of blood flow and platelet transport in pathological vessels. *Ann N Y Acad Sci* 2004; 1015(1): 351–366.
36. Ghodrati M, Maurer A, Schlöglhofer T, et al. The influence of left ventricular assist device inflow cannula position on thrombosis risk. *Artif Organs* 2020; 44: 939–946.
37. Rowlands GW and Antaki JF. High-speed visualization of ingested, ejected, adherent, and disintegrated thrombus in contemporary ventricular assist devices. *Artif Organs* 2020; 44: E459–E469.
38. Rossini L, Braun OÖ, Brambatti M, et al. Intraventricular flow patterns in patients treated with left ventricular assist devices. *ASAIO J* 2021; 67(1): 74–83.
39. Liao S, Simpson B, Neidlin M, et al. Numerical prediction of thrombus risk in an anatomically dilated left ventricle: the effect of inflow cannula designs. *Biomed Eng Online* 2016; 15(S2): 136.
40. Lewis RS, Wang L, Spinelli KJ, et al. Surgical occlusion of the left atrial appendage and thromboembolic complications in patients with left ventricular assist devices. *J Heart Lung Transplant* 2017; 36(5): 586–588.
41. Deshmukh A, Bhatia A, Sayer GT, et al. Left atrial appendage occlusion with left ventricular assist device decreases thromboembolic events. *Ann Thorac Surg* 2019; 107(4): 1181–1186.
42. Gaeta S, Dyverfeldt P, Eriksson J, et al. Fixed volume particle trace emission for the analysis of left atrial blood flow using 4D flow MRI. *Magn Reson Imaging* 2018; 47: 83–88.
43. Faludi R, Szulik M, D'hooge J, et al. Left ventricular flow patterns in healthy subjects and patients with prosthetic mitral valves: an in vivo study using echocardiographic particle image velocimetry. *J Thorac Cardiovasc Surg* 2010; 139(6): 1501–1510.
44. Collia D, Vukicevic M, Meschini V, et al. Simplified mitral valve modeling for prospective clinical application of left ventricular fluid dynamics. *J Comput Phys* 2019; 398: 108895.
45. Domenichini F and Pedrizzetti G. Asymptotic model of fluid-tissue interaction for mitral valve dynamics. *Cardiovasc Eng Technol* 2015; 6(2): 95–104.
46. Su B, Wang X, Kabinejadian F, et al. Effects of left atrium on intraventricular flow in numerical simulations. *Comput Biol Med* 2019; 106: 46–53.